



Coupled Au nanoclusters and silica spheres-coated carbon dots to engineer a ratio fluorescence strategy for on-site monitoring of chloroquine

Shun Wang^a, Yaqing Han^a, Mengke Wang^a, Junyang Chen^{c,*}, Xia Zhao^a, Haitao Han^a, Yuze Chen^d, Hao Wang^{a,*}, Guannan Wang^{b,*}

^a College of Medical Engineering, Jining Medical University, Jining 272067, PR China

^b School of Pharmacy, Shenyang Medical College, Shenyang 110034, PR China

^c School of Life Sciences, Zhengzhou University, Zhengzhou 450001, PR China

^d State Key Laboratory of Inorganic Synthesis and Preparative Chemistry, College of Chemistry, Jilin University, Changchun 130012, PR China

ARTICLE INFO

Keywords:

Ratio fluorescence sensor
Portable kit
Chloroquine
Au nanoclusters
Carbon dots

ABSTRACT

Accurate and timely detection of chloroquine (5-chloro-8-hydroxy-7-iodoquinoline, CQ) is crucial to prevent adverse effects from excessive or prolonged use. Herein, a core-satellite nanostructure of coupled Au nanoclusters and silica spheres-coated carbon dots (AuNCs/CDs@SiO₂) was designed, achieving the high fluorescence (FL) efficiency of AuNCs. Consequently, a ratio fluorescent sensing platform was established for the first time to detect CQ sensitively, which was designed by applying the FL signal of CDs as a reference to provide a built-in correction and the AuNCs immobilized on the SiO₂ as an analytical tag. By the design of the fluorescence quenching of Cu²⁺ on AuNCs and CQ-induced fluorescence recovery due to the strong complexation of CQ toward Cu²⁺, a AuNCs/CDs@SiO₂ based ratio fluorescent probe can realize highly selective differentiation and accurate analysis of CQ, with a limit of detection (LOD) of 89.2 nM. Additionally, this sensor platform was utilized to detect CQ in commercial cream, human serum and urine samples with preferable analytical performance. Additionally, this sensing platform was fabricated into a portable test kit to provide an intelligent detection method for on-site monitoring of CQ with the aid of a smartphone-assisted homemade 3D-printing portable device. This study is expected to provide useful insight into understanding the formation of core-satellite nanostructure to encourage applications in the development of powerful biosensors for accurate drug monitoring.

1. Introduction

Chloroquine (5-chloro-8-hydroxy-7-iodoquinoline, CQ), as a widely used medication in the pharmaceutical field, possesses multiple pharmacological functions, including antifungal, antiparasitic, antiviral, and anti-inflammatory properties [1–3]. In recent years, CQ has attracted interest as a possible therapeutic option for neurodegenerative diseases, including Parkinson's, Alzheimer's, and Huntington's diseases [4,5]. However, prolonged or excessive use of CQ can lead to serious toxic effects such as neurotoxicity and cytotoxicity, and it has been associated with diseases like subacute myelo-optic neuropathy (SMON) syndrome [6,7]. Accurate detection of the concentration of CQ in medications enables timely monitoring of patient's medication usage, avoiding adverse reactions caused by excessive or long-term use of the drug. Accordingly, establishing simple, fast, and accurate methods for

detecting CQ is crucial for mitigating its adverse consequences.

Previous literature reports have outlined several detection methods for CQ, including electrochemical [8], colorimetric [9], fluorescence (FL) [10], and high-performance liquid chromatography (HPLC) [11] techniques. Nanomaterial-assisted construction of fluorescent sensors, in particular, have gained prominence as effective alternatives, boasting higher sensitivity, accessibility, cost-effectiveness, rapid analysis, and the ability to provide real-time detection within situational analysis. Recently, carbon dots [12], sulfur quantum dots [10], gold nanoclusters [13] based fluorescence sensing platform have been innovatively proposed for CQ. However, these assays rely solely on a single fluorescence signal change and may be prone to interference from uncontrollable factors such as probe concentrations, photobleaching, and changes in environmental conditions [14,15]. To overcome the difficulties faced by single-emission fluorescent sensor, the use of a ratio fluorescent (RF)

* Corresponding authors.

E-mail addresses: junyuchen@zzu.edu.cn (J. Chen), wanghao20220819@mail.jnmc.edu.cn (H. Wang), chemwangguannan@126.com (G. Wang).

<https://doi.org/10.1016/j.snb.2024.137090>

Received 13 June 2024; Received in revised form 17 November 2024; Accepted 5 December 2024

Available online 6 December 2024

0925-4005/© 2024 Published by Elsevier B.V.

sensing strategy is the most effective solution by utilize multiple fluorescence output signals as detection indicators with the built-in self-calibration function [16–19]. However, the absence of efficient functional nanomaterials and sensor mechanism designs has hindered the development of RF strategies for CQ. Therefore, it is imperative to develop efficient functional nanomaterials-based ratio fluorescence methods for determination of CQ.

The construction of ratio fluorescent sensor is the cornerstone in the development of ratio sensing methods. Notably, constructing ratio fluorescent probes by combining the superior properties of different fluorescent nanomaterials is an effective approach for achieving efficient sensing [20]. For example, metal organic frameworks (MOFs) encapsulated quantum dots (QDs) nanocomposites [21] and nanoclusters/poly-dopamine nanoparticles [22] have been projected for biomedical sensing. In recent advancements, fluorescent carbon dots (CDs) have emerged as a viable alternative to traditional fluorophores within the realm of bioimaging and biosensing [23,24]. Their appeal lies in their notable attributes, such as heightened photostability, resilience against photobleaching and blinking, chemical inertness, improved capacity for surface grafting, and exceptional biocompatibility [25,26]. Similarly, there has been a surge of interest in fluorescent gold nanoclusters (AuNCs), primarily due to their facile synthesis, favorable water solubility, environmentally friendly characteristics, and cost-effectiveness [27,28]. Attributable to these myriad benefits, AuNCs have assumed pivotal roles in the realms of medical diagnostics and biochemical assays [29–31]. The exceptional properties exhibited by AuNCs and CDs provide valuable inspiration for the development of CDs and AuNCs combined ratio sensors.

Enlightened by the above merits, herein, a core-satellite nanostructure of AuNCs/CDs@SiO₂ nanohybrid was strategically constructed through a facile method, and a AuNCs/CDs@SiO₂-based RF platform was rationally constructed for biosensing of CQ for the first time (Scheme 1). Meanwhile, ideally, the immobilization of SiO₂ boosted the FL property of AuNCs. Based on the high fluorescence efficiency of AuNCs and the high stability of CDs in the AuNCs/CDs@SiO₂, a novel RF strategy was developed for CQ detection by employing AuNCs as the response unit and CDs as the reference unit. Additionally, a hydrogel kit immobilized with AuNCs/CDs@SiO₂ was developed for CQ via a

smartphone-assisted homemade 3D-printing portable device, offering significant advantages for equipment-free and visual detection of CQ.

2. Experimental section

2.1. Fabrication of AuNCs/CDs@SiO₂ composite

Preparation procedures for CDs@SiO₂ and AuNCs were shown in the Supporting Material. For the preparation of AuNCs/CDs@SiO₂, 3.0 mg CDs@SiO₂ was added into 8.5 mL H₂O and then treated by sonication for 15 min. Then, AuNCs (1 mL, 1.0 mg/mL) and Tris-HCl buffer solution (pH=6.0, 0.5 mL, 100 mM) were introduced into the above solution. The combined solution was permitted to react for 2 h at room temperature. Subsequently, the prepared AuNCs/CDs@SiO₂ was collected by centrifugation (9000 r/min, 10 min) and washed with H₂O for 3 times. Finally, the product was redispersed in 10 mL H₂O for the following use.

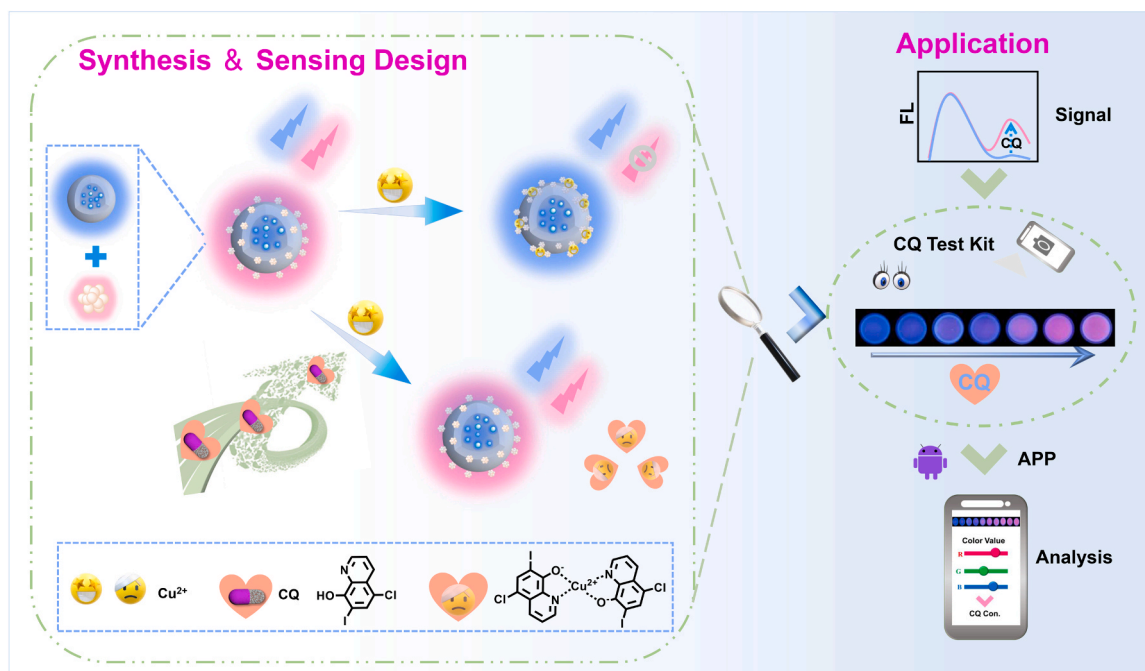
2.2. Fluorescent detection of CQ

To detect CQ, Cu²⁺ solution (200 μL, 0.1 mM) was reacted with different concentrations of CQ at 25 °C for 40 min. Then, AuNCs/CDs@SiO₂ (500 μL, 0.4 mg/mL) were added to the above mixtures. After 10 min, the fluorescence spectra were recorded with a 365 nm excitation wavelength.

2.3. Fabrication and application of a portable kit for CQ

Briefly, 40 mg agarose was added to 4.0 mL H₂O and heated until dissolved. When the mixed solution was cooled to 50 °C, AuNCs/CDs@SiO₂ (4.0 mL, 0.4 mg/mL) was added to it. After pouring the above mixture into the centrifuge tube cap and cooling, the AuNCs/CDs@SiO₂ agar gel was obtained.

For detection of CQ by using the prepared kit, CQ and Cu²⁺ were added to the interior of the EP tube and reacted at 25 °C for 40 min. Then, the tube was inverted to allow the reacted solution to infiltrate into the agarose hydrogel containing AuNCs/CDs@SiO₂. After the reaction, the EP tube caps were removed and placed in a 3D-printing box,



Scheme 1. The AuNCs/CDs@SiO₂-based on-site CQ monitoring.

and the optical images of the test kit were captured using a smartphone (vivo s15). And the RGB data of the optical photos were analyzed by the Color-Collection APP.

2.4. Real samples analysis of CQ

Two commercially available CQ creams bought from JD shopping mall were selected as the actual samples for CQ analysis. The creams were diluted 100 times to bring their content within the linear detection

range of this assay, and then filtered with 0.22 μm filter membranes. Additionally, CQ analysis was performed on serum and urine samples that were voluntarily provided by informed participants. Initially, the collected samples were filtered using a 0.45 μm filter membrane to eliminate particulate matter. Subsequently, the samples were subjected to centrifugation at a speed of 12,000 r/min for 20 min to enhance their purity prior to analysis. Finally, the content of CQ in real samples was detected via a standard addition method by following the procedures in Section 2. 2.

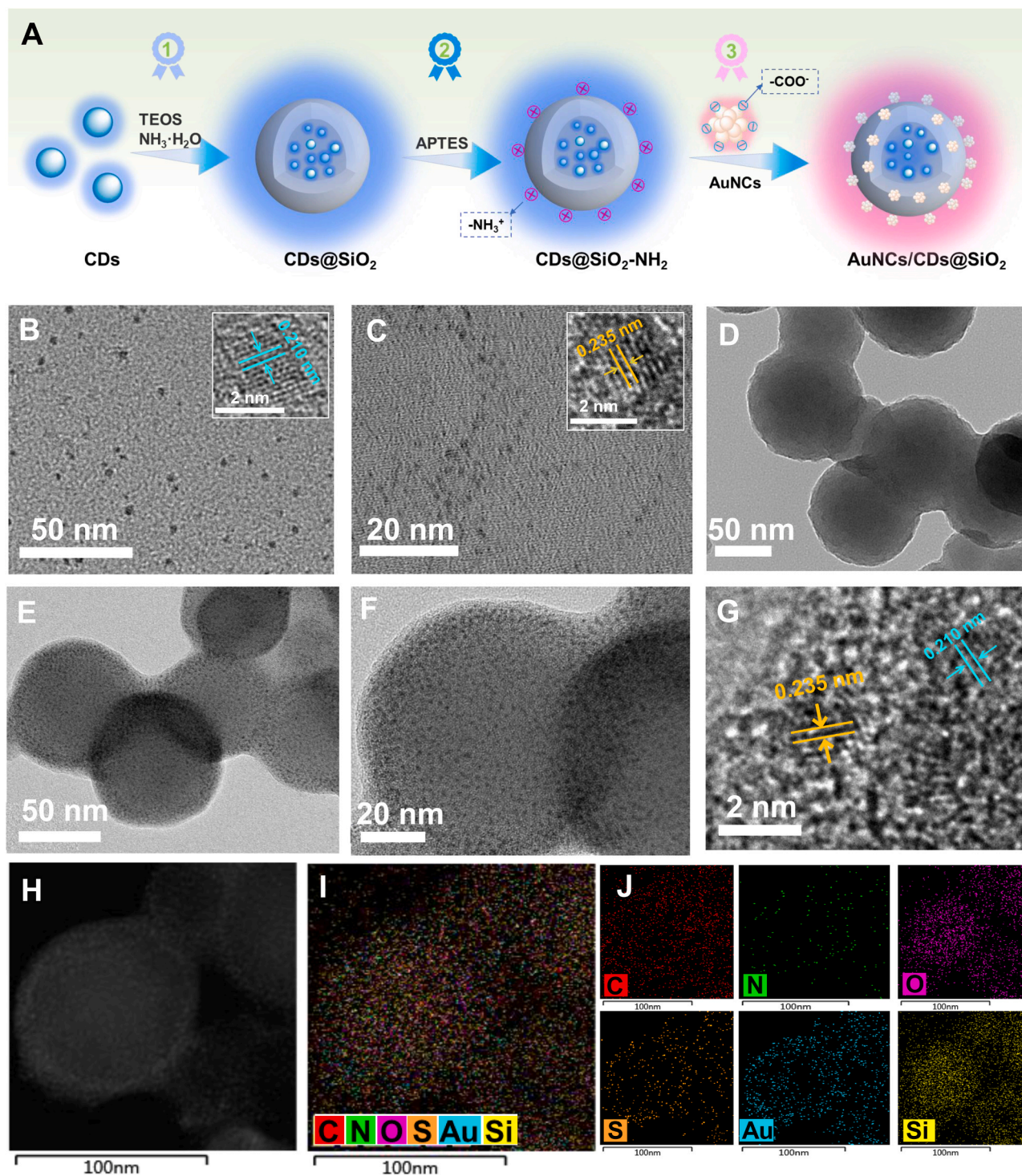


Fig. 1. (A) Diagram of the synthesis of AuNCs/CDs@SiO₂. TEM images of CDs (B), AuNCs (C), CDs@SiO₂ (D), and AuNCs/CDs@SiO₂ (E-F). HR-TEM images of CDs (B, insert), AuNCs (C, insert) and AuNCs/CDs@SiO₂ (G). (H-J) STEM image and elemental mappings (C, N, O, S, Au, and Si) for AuNCs/CDs@SiO₂.

3. Results and discussion

3.1. Preparation and characterization of the materials

The AuNCs/CD@SiO₂ nanocomposites were designed by a three-step process (Fig. 1A). (1) The CDs@SiO₂ composite was synthesized by encapsulating CDs in SiO₂ spheres through a Stöber method. (2) The CDs@SiO₂ composite was treated by surface modification with APTES to prepare the aminated CDs@SiO₂ spheres. (3) The AuNCs noncovalently bound to the CDs@SiO₂ surface through electrostatic interaction to obtain the AuNCs/CDs@SiO₂-based ratio fluorescent probe.

The CDs, AuNCs, CDs@SiO₂ and AuNCs/CDs@SiO₂ were firstly systematically studied by the TEM characterizations. Fig. 1B showed the CDs displayed good mono-dispersity with the average particle diameter of 3.58 nm (Fig. S1). The insert in Fig. 1B of HR-TEM image displayed that the crystal lattice fringe (0.210 nm) of CDs, which was agreed with that of in-plane lattice spacing of graphene (100 facet) [32]. Besides, Fig. 1C and Fig. S2 showed the TEM image of AuNCs, in which uniform particles were observed with an average diameter size of 2.02 nm. The insert in Fig. 1C of HR-TEM image displayed that the crystal lattice fringe (0.235 nm) of AuNCs, which was corresponded to the (111) lattice spacing of face centered cubic Au [33,34]. From Fig. 1D, after the

being embedded in SiO₂ spheres, the CDs@SiO₂ displayed a round morphology similar as SiO₂ with an average diameter of around 90 nm. As revealed in Fig. 1E, after the assembly of AuNCs on CDs@SiO₂, AuNCs/CDs@SiO₂ kept a similar spherical morphology as CDs@SiO₂. The SEM image in Fig. S3 also showed that the AuNCs/CDs@SiO₂-based nanomaterial displayed a uniform size and good dispersion. From the magnified TEM image of AuNCs/CDs@SiO₂ in Fig. 1F and Fig. 1H, it can be clearly observed that the AuNCs as bright dots evenly distributed within the CDs@SiO₂ matrix, and the (111) lattice spacing from AuNCs as well as (100) lattice spacing from CDs can be observed. Additionally, the EDS elemental mapping in Fig. 1I and 1J showed the C, N, O, S, Au, and Si elements in the AuNCs/CDs@SiO₂. The EDX spectrum presented in Fig. S4 provided further evidence that the composition of the AuNCs/CDs@SiO₂ structure includes C, N, O, S, Au, and Si. Meanwhile, the amounts of Si and Au in AuNCs/CDs@SiO₂ were 32.86 % and 17.52 % (weight %). These findings verified the as-prospected preparation of AuNCs/CDs@SiO₂.

The analysis of Fig. 2A and B revealed the charged property properties of the prepared nanomaterials. Briefly, CDs, AuNCs, and AuNCs/CDs@SiO₂ demonstrated the characteristic negative charges, contrasting with the positive charges observed for SiO₂ and CDs@SiO₂. The zeta potentials of SiO₂ and CDs were measured to be +21.0 mV and

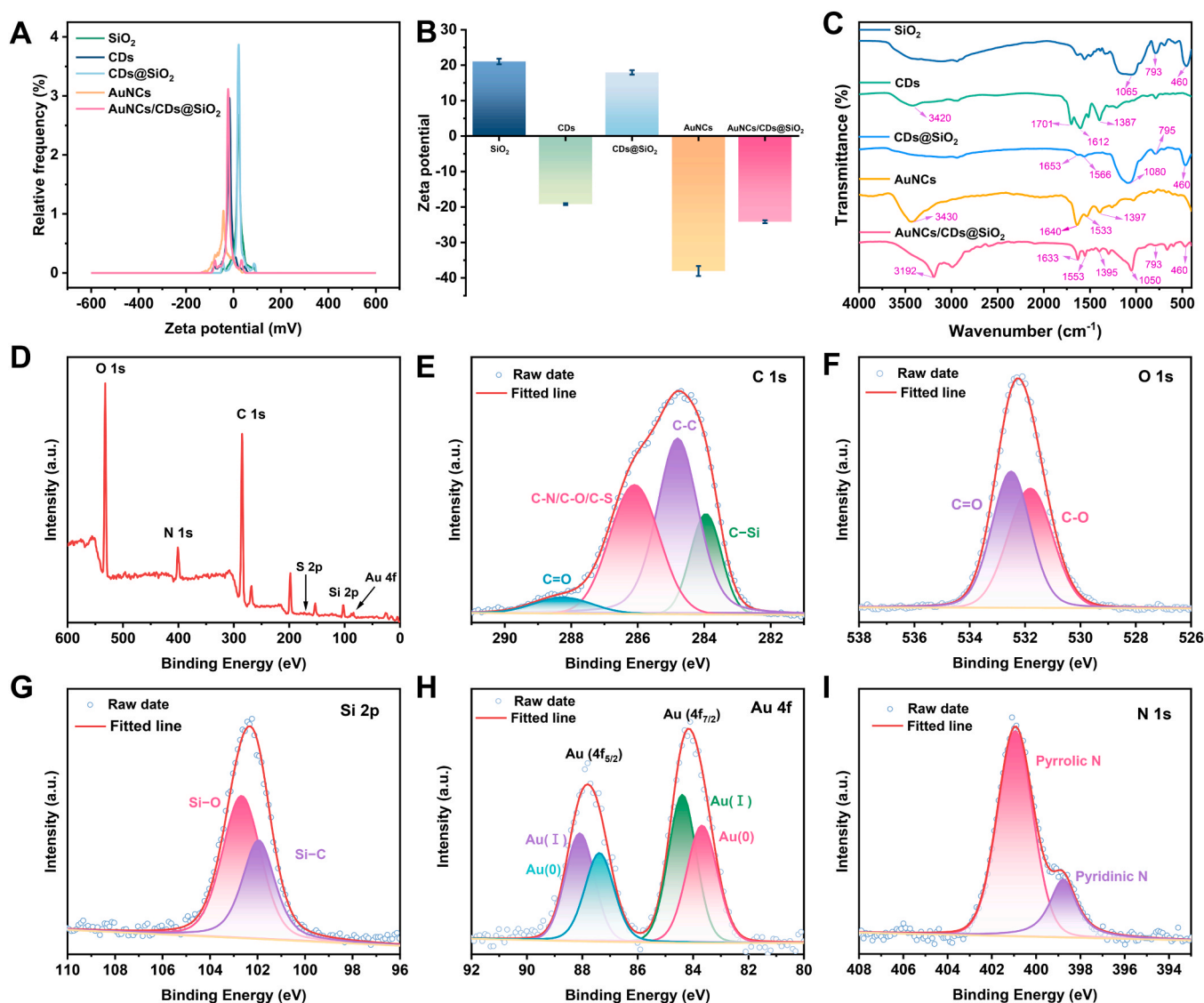


Fig. 2. Zeta potentials results (A, B) and FT-IR spectra (C) of SiO₂, CDs, CDs@SiO₂, AuNCs, and AuNCs/CDs@SiO₂, respectively. (D) XPS spectrum of AuNCs/CDs@SiO₂. The high-resolution XPS spectra of C 1s (E), O 1s (F), Si 2p (G), Au 4f (H), and N 1s (I), respectively.

−19.2 mV, respectively. Notably, the encapsulation of CDs within SiO₂ resulted in the surface of CDs@SiO₂ manifesting the electric characteristics of SiO₂, registering a potential of + 18.0 mV. With a zeta potential of −38.1 mV, AuNCs were effectively sequestered onto the positively charged surface of CDs@SiO₂ by electrostatic interactions, facilitating the formation of AuNCs/CDs@SiO₂ composite probes. This synergistic interaction is further evidenced by the observed increase in zeta potential (−24.2 mV) upon the amalgamation of AuNCs with CDs@SiO₂, unequivocally indicating the successful synthesis of AuNCs/CDs@SiO₂.

The characterizations of SiO₂, CDs, CDs@SiO₂, AuNCs, and AuNCs/CDs@SiO₂ were conducted using FT-IR spectroscopy. As illustrated in Fig. 2C, the strong peak observed at around 1083 cm^{−1} corresponded to the anti-symmetric stretching vibration of Si–O–Si bonds. Two characteristic peaks observed around 793 cm^{−1} to 1460 cm^{−1} were attributed to the symmetric and bending vibrations of Si–O bonds [35]. In the FT-IR spectrum of CDs, a peak is observed at 3420 cm^{−1}, indicating stretching vibrations of N–H or O–H bonds. Peaks at 1701 cm^{−1} corresponded to the bending vibration of N–H, while those at 1612 cm^{−1} and 1387 cm^{−1} indicate stretching vibrations of C=O and C–N bonds, respectively [36]. These findings confirmed the successful synthesis of CDs. Upon the formation of CDs@SiO₂, several absorption peaks were observed. Peaks at 1653 cm^{−1} and 1566 cm^{−1} were attributed to the stretching vibration of C=O and the bending vibration of N–H, respectively. Peaks observed at 1080 cm^{−1}, 795 cm^{−1}, and 460 cm^{−1} corresponded to the stretching and bending vibrations of Si–O bonds. These results demonstrated the successful embedding of CDs into amino-modified SiO₂ spheres. Additionally, in the FT-IR spectrum of AuNCs, characteristic peaks were observed at 1397 cm^{−1} (C–O stretching vibration), 1640 cm^{−1} (C=O stretching vibration), 1533 cm^{−1} (N–H stretching vibration), and 3430 cm^{−1} (O–H stretching vibration) [37]. Upon the formation of AuNCs/CDs@SiO₂, specific absorption peaks from SiO₂, CDs, CDs@SiO₂, and AuNCs were observed, indicating the successful preparation of the AuNCs/CDs@SiO₂ composite probe.

The electronic structure and surface elemental composition of

AuNCs/CDs@SiO₂ were probed using XPS. In Fig. 2D, distinct peaks at 285 eV (C 1 s), 401 eV (N 1 s), 532 eV (O 1 s), 102 eV (Si 2p), 88 eV/84 eV (Au 4f), and 165 eV (S 2p) were evident. Fig. 2E illustrated the high-resolution C1s spectrum, revealing diverse structural components: C–Si (284.0 eV), C–C (284.8 eV), C–N/C–O/C–S (286.1 eV), and C=O (288.3 eV) [32,38]. In the O 1 s spectrum (Fig. 2F), peaks attributed to C–O (531.8 eV) and C=O (532.5 eV) are discernible. The Si 2p spectrum (Fig. 2G) displayed peaks at 102.0 eV and 102.7 eV, assigned to Si–C and Si–O, respectively [38]. Notably, Au (Fig. 2H) exhibited distinctive signals: Au 4f_{7/2} (84.4 eV) and Au 4f_{5/2} (88.1 eV) for Au(I), and Au 4f_{5/2} (87.4 eV) and Au 4f_{7/2} (83.7 eV) for Au(0) [39]. The contents of Au(I) and Au(0) in all Au atoms in the AuNCs were determined to be 52.9 % and 47.1 %, respectively. The N 1 s spectrum (Fig. 2I) exhibited peaks corresponding to pyridinic N (398.78 eV) and pyrrolic N (401.0 eV) [38,40]. The S 2p spectrum (Fig. S5) showed three peaks indicative of oxidized S (168.6 eV), -SH (162.2 eV), and Au–S (163.4 eV) [41,42]. These results provided crucial insights into the intricate surface chemistry and electronic properties of AuNCs/CDs@SiO₂.

3.2. Fluorescence property of the AuNCs/CDs@SiO₂ composite

A comprehensive study was conducted to reveal the fluorescence properties of AuNCs/CDs@SiO₂. Firstly, Fig. 3A showed a schematic diagram of the combination of CDs, AuNCs, and SiO₂. In Fig. 3B, after the assembly to be AuNCs/CDs@SiO₂, the blue fluorescence of CDs diminished, while the red fluorescence of AuNCs intensified. As depicted in Fig. 3B insert, the resultant AuNCs/CDs@SiO₂ exhibited a distinctive pink fluorescence. The CIE chromaticity diagrams presented in Fig. 3C further corroborated the influence of complexation on the fluorescence color. The mechanism underlying the fluorescence performance changes of CDs and AuNCs was further investigated during the construction of the ratio probe. Firstly, we explored the reason for the decrease in fluorescence upon CDs' complexation with AuNCs. In Fig. 3D, it can be observed that the emission spectrum of carbon dots overlaps well with the UV absorption spectrum of AuNCs, indicating the possible

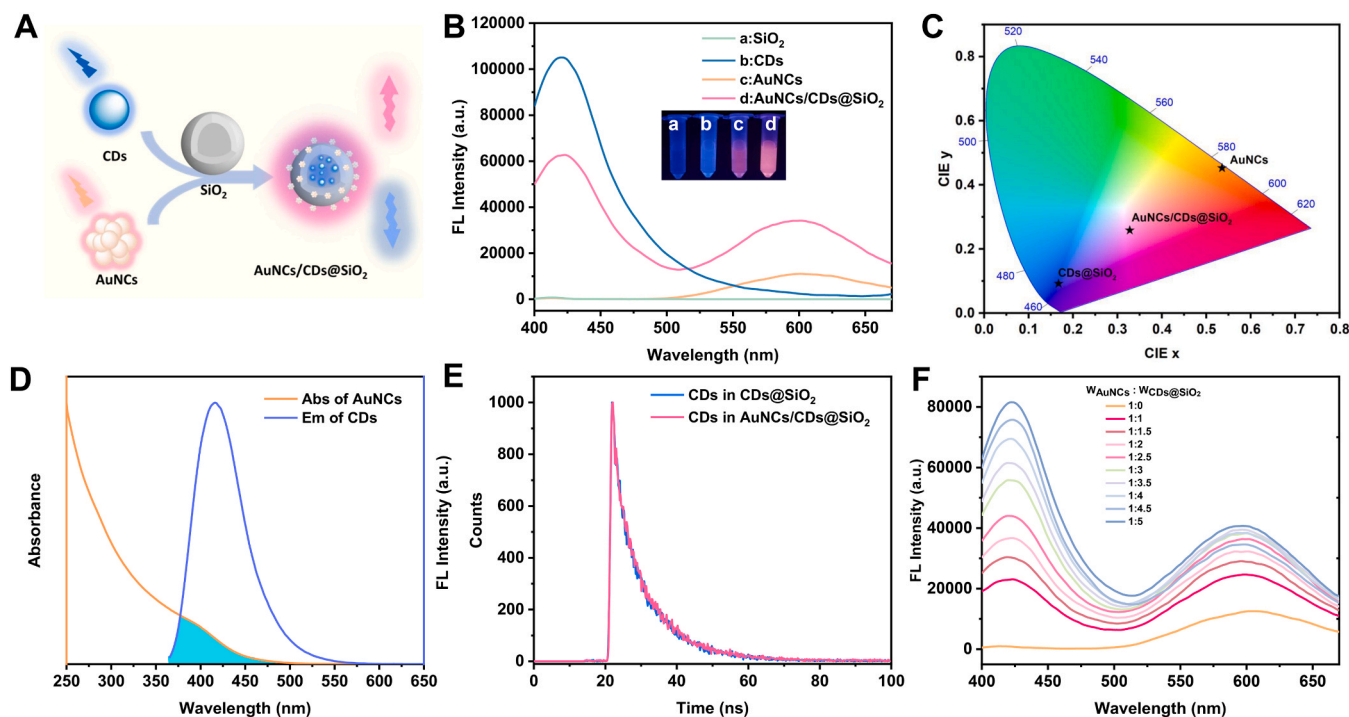


Fig. 3. (A) Diagram of the synthesis process of AuNCs/CDs@SiO₂. (B) FL emission spectra of SiO₂, CDs, AuNCs, and AuNCs/CDs@SiO₂. (C) CIE chromaticity charts of CDs@SiO₂, AuNCs, and AuNCs/CDs@SiO₂. (D) UV absorption spectrum of AuNCs and FL emission spectrum of CDs, respectively. (E) The fluorescence lifetime of CDs in CDs@SiO₂ and AuNCs/CDs@SiO₂, respectively. (F) FL emission spectra of AuNCs/CDs@SiO₂ at varied ratios (weight: weight) of AuNCs to CDs@SiO₂.

occurrence of either induced fluorescence energy transfer (IFE) or fluorescence resonance energy transfer (FRET) between them [43]. Subsequently, the results of lifetime tests showed that the lifetimes of CDs before and after complexation with AuNCs remained almost unchanged (Fig. 3E and Table S1), suggesting the absence of an energy transfer process between them (Fig. 3E). The fluorescence of CDs was quenched by AuNCs through the IFE effect [44]. On the other hand, after the immobilization of AuNCs on SiO₂ nanoparticles, the FL of AuNCs was increased, which could be attributed to the reasons that the confinement effect of SiO₂ can suppress the intramolecular motion and reduce the non-radiative transitions of AuNCs, thus promoting the fluorescence of AuNCs [45,46]. This observation was also in accord with the previous reported regulatory confinement and aggregation-induced emission (AIE) characteristic of glutathione-coated AuNCs by the varied media materials [47–49].

Additionally, Fig. 3F elucidated the correlation between the fluorescence enhancement of AuNCs and the weight ratio (w/w) of AuNCs and CDs@SiO₂. Fig. S7A illustrated that as the content of CDs@SiO₂ increases, the fluorescence intensity of AuNCs showed a gradual augmentation. At a ratio of AuNCs to CDs@SiO₂ of 1:3 (w/w), the fluorescence intensity of AuNCs reached a plateau. Remarkably, this

value was thrice the original fluorescence intensity of AuNCs, and the fluorescence quantum yield (QY) was increased to 5.30 % compared to AuNCs (QY = 2.65 %).

Furthermore, the assembly conditions for the composite of AuNCs and CDs@SiO₂ were optimized. According to the results shown in Fig. S7B, it can be found that pH 6.0 was favorable for the composite of AuNCs and CDs@SiO₂. On the other hand, as displayed in Fig. S7C, the fluorescence intensity of AuNCs and CDs@SiO₂ stabilized within 1 h after composite formation. The stability of AuNCs/CDs@SiO₂ was examined. As depicted in Fig. S8A, AuNCs/CDs@SiO₂ showed minimal changes across various salt concentrations. In Fig. S8B, following 60 min of Xe lamp irradiation, CDs and AuNCs retained 99.8 % and 97.0 % of their initial intensities, respectively. These results signify a notable stability of both CDs and AuNCs after electrostatic composite formation. This advancement further enhances the potential applications of AuNCs/CDs@SiO₂, particularly in the realm of biosensing.

3.3. Construction of sensing platform

As illustrated in Fig. 4A, based on its excellent fluorescence performance, a CQ ratio fluorescence sensor based on AuNCs/CDs@SiO₂ was

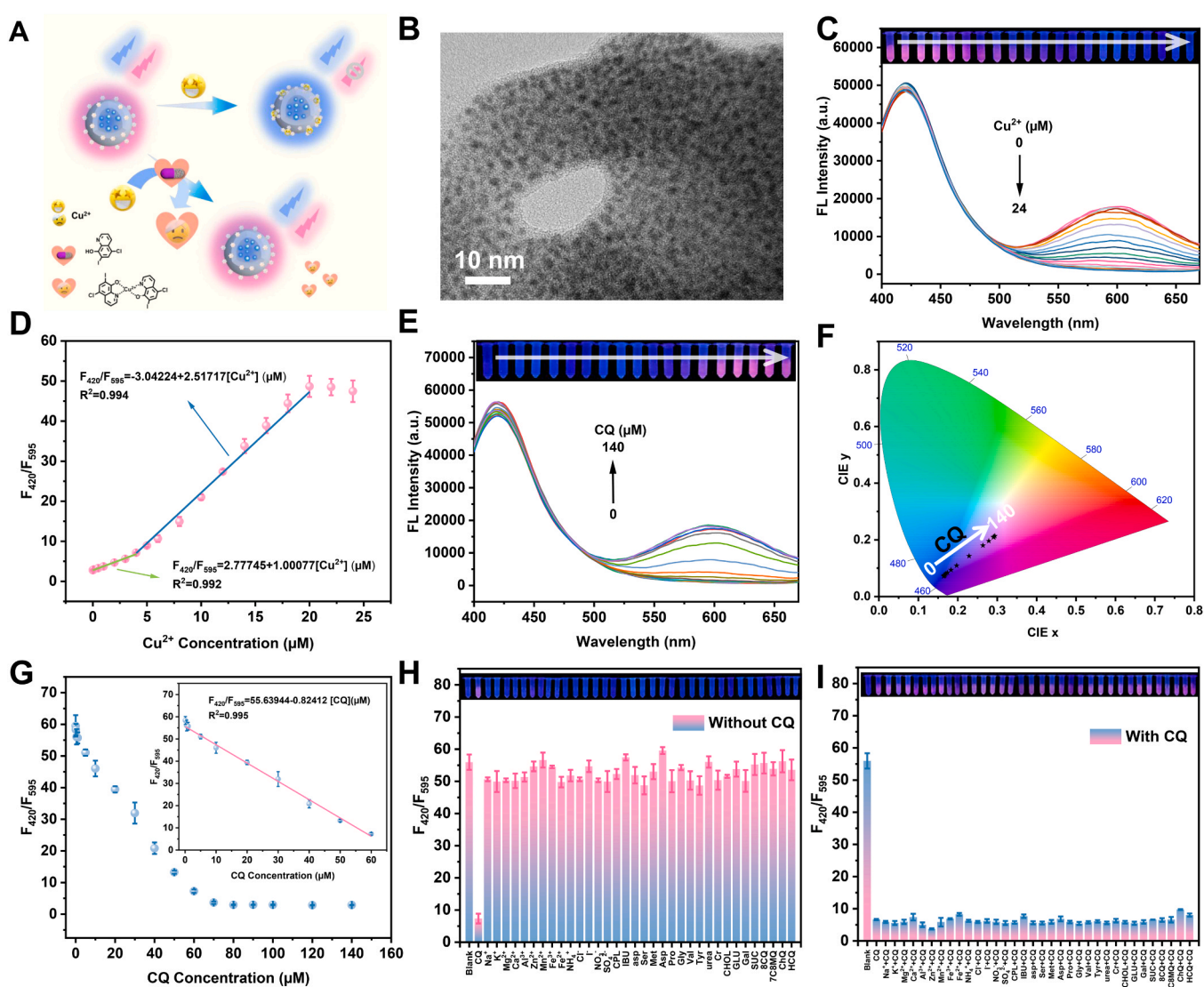


Fig. 4. (A) Diagram of the RF platform for CQ detection based on AuNCs/CDs@SiO₂. (B) TEM image of AuNCs/Cu²⁺ system. (C) FL spectra, and (D) intensity of AuNCs/CDs@SiO₂ with different Cu²⁺. (E) FL spectra, (F) chromaticity diagram, and (G) intensity of AuNCs/CDs@SiO₂ /Cu²⁺ system with different CQ concentration. Selectivity (H), and anti-interference ability (I) of the AuNCs/CDs@SiO₂-based assay for CQ.

developed. Firstly, Cu^{2+} can bind to the carboxyl groups of AuNCs to quench the fluorescence of AuNCs in the AuNCs/CDs@SiO₂. According to previous reports, the fluorescence quenching mechanism of AuNCs regulated by Cu^{2+} involves the coordination of Cu^{2+} with the carboxyl groups of the GSH ligand present on the surface of AuNCs, leading to the formation of Cu^{2+} @AuNCs complexes. These complexes may hinder the ligand-to-Au charge transfer process and facilitate an effective charge transfer from AuNCs to Cu^{2+} [50,51]. As shown in Fig. 4B, upon the addition of Cu^{2+} , significant aggregation of AuNCs was observed compared to the dispersed AuNCs in the absence of Cu^{2+} , confirming the binding of Cu^{2+} to AuNCs. Secondly, Cu^{2+} can react with CQ to generate CQ-Cu-CQ complexes, thereby inhibiting the quenching of AuNCs fluorescence by Cu^{2+} . As revealed in Fig. S9, compared with CQ and Cu^{2+} , the CQ/ Cu^{2+} system displayed a new absorption peak at around 420 nm with the obvious yellow appearance of the solution, suggesting the complexation of CQ toward Cu^{2+} . Meanwhile, CDs were encapsulated in SiO₂, ensuring their fluorescence remained unaffected during the process. Therefore, this detection platform utilized the fluorescence changes of AuNCs as the response signal, with CDs serving as the reference signal, enabling rapid, convenient, and sensitive ratio fluorescence detection of CQ by measuring the fluorescence intensity ratio (F_{420}/F_{595}).

Based on the aforementioned mechanism, this ratio fluorescence sensing platform can be utilized for the detection of Cu^{2+} , and the detection performance for Cu^{2+} directly impacted the sensitivity of CQ detection. Initially, the time for Cu^{2+} to quench the fluorescence of AuNCs/CDs@SiO₂ was optimized, as depicted in Fig. S10. After a reaction time of 10 min, the fluorescence intensity ratio (F_{420}/F_{595}) stabilized, indicating that the reaction had reached equilibrium. At this reaction time, we evaluated the analytical performance of AuNCs/CDs@SiO₂ towards Cu^{2+} . As shown in Fig. 4C, as the Cu^{2+} concentration increased from 0 to 24 μM , the fluorescence of AuNCs/CDs@SiO₂ at 595 nm gradually decreased, while the fluorescence at 420 nm remained relatively constant. Fig. 4D illustrates that the fluorescence intensity ratio of AuNCs/CDs@SiO₂ displayed an increasing trend, with a good linear correlation with Cu^{2+} concentration within certain ranges. For Cu^{2+} concentrations ranging from 0.005 to 4 μM , the linear equation was: $F_{420}/F_{595} = 2.77745 + 1.00077[\text{Cu}^{2+}]$ (μM), with an R^2 value of 0.992; for Cu^{2+} concentrations ranging from 4 to 20 μM , the linear equation was: $F_{420}/F_{595} = -3.04224 + 2.51717[\text{Cu}^{2+}]$ (μM), with an R^2 value of 0.994. The limit of detection (LOD) of Cu^{2+} was 0.00429 μM (4.29 nM). These results demonstrate the high sensitivity of this ratio fluorescence sensing platform for Cu^{2+} detection, which also enabled the sensitivity of Cu^{2+} -mediated CQ assay.

The feasibility of this method for detecting CQ was further validated. Above all, Fig. S11 showed that CQ had not affect the fluorescence of AuNCs, CDs@SiO₂ or AuNCs/CDs@SiO₂, ensuring the specificity of Cu^{2+} -mediated sensing strategy. Fig. S12 described the addition of Cu^{2+} effectively quenched the AuNCs fluorescence in AuNCs/CDs@SiO₂, whereas the fluorescence of AuNCs remained unaffected when the Cu^{2+} /CQ was added. The fluorescence of CDs in the AuNCs/CDs@SiO₂ kept unaffected during the process. The above results indicated the feasibility of this ratio fluorescent assay by employing the fluorescence of AuNCs as response signal and CDs as reference signal in the engineered AuNCs/CDs@SiO₂. Under the verified optimal experimental conditions in Fig. S13, the fluorescence emission spectroscopy on the Cu^{2+} /AuNCs/CDs@SiO₂ system containing different concentrations of CQ was conducted. Fig. 4E described the fluorescence of AuNCs/CDs@SiO₂ at 595 nm gradually increased as the CQ concentration ranged from 0 to 140 μM , while the fluorescence at 420 nm remained relatively constant. The chromaticity diagram of AuNCs/CDs@SiO₂ in Fig. 4F further confirmed this trend. Consequently, the fluorescence intensity ratio of AuNCs/CDs@SiO₂ exhibited a decreasing trend (Fig. 4G), and within the CQ concentration range of 0.1–60 μM , it demonstrated a good linear relationship with a correlation coefficient of $R^2 = 0.995$. A linear regression equation was determined to be $F_{420}/$

$F_{595} = 55.63944 - 0.82412 [\text{CQ}]$ (μM). The LOD of CQ was 0.0892 μM (89.2 nM). Besides, by referring to a previous method [52], five parallel experimental samples containing CQ with a final concentration of 0.1 μM , 1 μM and 10 μM were prepared for the reproducibility experiment, and the relative standard deviations (RSDs) of 3.42 %, 2.41 %, and 2.67 %, respectively, were obtained, which were less than 5 % and indicated the good reproducibility of this method on CQ detection.

Selective recognition and anti-interference ability are crucial indicators for assessing the practicality of a sensing platform, especially in complex biological samples. Therefore, to simulate the practical application environment of CQ detection, The selectivity and anti-interference ability of the fluorescence sensors were systematically evaluated in the presence of common interfering substances, including ions (Na^+ , K^+ , Mg^{2+} , Mn^{2+} , Ca^{2+} , Al^{3+} , Zn^{2+} , Fe^{3+} , Fe^{2+} , NH_4^+ , Cl^- , I^- , NO_3^- , and SO_4^{2-}), other common drugs (chloramphenicol (CPL), ibuprofen (IBU), and aspirin (ASP)), amino acids (serine (Ser), methionine (Met), aspartic acid (Asp), proline (Pro), glycine (Gly), valine (Val), and tyrosine (Tyr)), other biomolecules (urea, creatinine (Cr), cholesterol (CHOL), glucose (GLU), galactose (Gal), and sucrose (SUC)), and CQ-like compounds (structures shown in Fig. S14, 8-chloroquinoline (8CQ), 7-chloro-8-methylquinoline (7C8MQ), chloroquine (ChQ), and hydroxychloroquine (HCQ)). Fig. 4H described that the fluorescence intensity ratio (F_{420}/F_{595}) of the system decreased significantly only in the presence of CQ. In the absence of CQ, there was no noticeable change in the fluorescence intensity ratio (F_{420}/F_{595}), indicating high selectivity of the sensing system towards CQ. Furthermore, interference experiments were conducted by adding the aforementioned substances in the presence of CQ. Fig. 4I depicted the fluorescence signal response of the sensing platform to CQ remained essentially the same before and after the addition of interfering substances, demonstrating the excellent anti-interference ability of the CQ sensing platform.

3.4. The preparation and application of portable test kits

Based on the above study, the development of a CQ test kit by encapsulating AuNCs/CDs@SiO₂ in agarose hydrogel was conducted (Fig. 5A). The stability of the hydrogel was first discussed. Regardless of exposure to UV light for 1 h (Fig. S15) or storage for up to 1 month (Fig. S16), the fluorescence color of the hydrogel remained largely unaffected, revealing the good photostability and storage stability. Therefore, this hydrogel kit loaded with AuNCs/CDs@SiO₂ was suitable for preparing portable test kits and further applied for CQ detection combined with a homemade 3D-printing portable device. In Fig. 5B, it can be observed that the color of the agarose test kit changes significantly with increasing CQ concentration. Subsequent digital image processing using color-picking software allowed the plotting of the quantitative curve of RGB values against CQ concentration (Fig. 5C). Within the range of CQ concentrations from 5 to 80 μM , a good linear relationship is observed between the (R+G)/B value and CQ concentration ($R^2 = 0.997$). These findings suggested that the portable kit provided a intuitive and easily transportable on-site quantitative tool for CQ.

3.5. Testing of CQ in the commercial creams

To evaluate the accuracy of the established method in detecting actual samples, we selected two commercially available creams, human serum and urine to assess the practical application value of this assay. As shown in Fig. S17, the two creams, human serum and urine did not affect AuNCs/CDs@SiO₂ themselves. Firstly, the creams were diluted 100 times to bring their content within the linear detection range of this assay. CQ contents in the two un-spiked creams (100-time diluted) were detected to be 15.38 μM and 15.34 μM by this method, which were calculated as 3.13 % and 3.12 % (by weight) in the original creams, respectively. Besides, a colorimetric method was employed for CQ detection as a comparison (Fig. S18). CQ contents in the two un-spiked

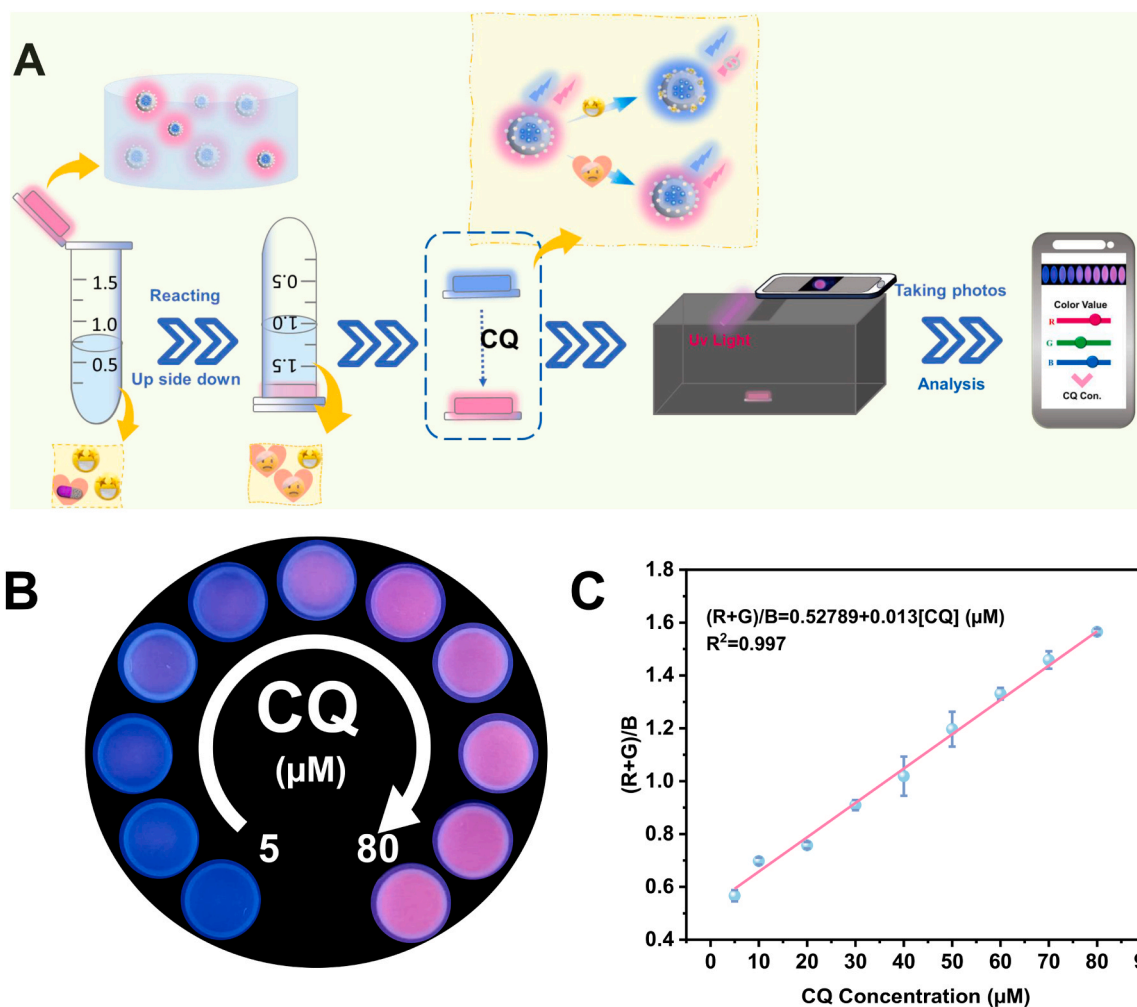


Fig. 5. (A) Diagram of the procedures for CQ detection by the portable kit. (B) Images of hydrogel at varied CQ concentrations under a 365 nm UV light. (C) Linearity between (R+G)/B value and the CQ concentration.

creams (100-time diluted) were detected to be 14.62 and 15.07 μM by the colorimetric method, which were calculated as 2.98 % and 3.07 % (by weight) in the original creams, respectively. The results were consistent with the reported content of 3 % (by weight) in the cream's instructions, confirming the accuracy of our method. Secondly, we further determined the CQ in the creams using the standard addition method. From the obtained data table (Table S2), the recovery rate of CQ ranged from 101.2 % to 102.8 %, with the RSD less than 3.7 %. Besides, as for the human serum and urine samples, the recovery rate of CQ ranged from 101.3 % to 109.1 %, with the RSD less than 3.9 % (Table S2). The results indicate that the ratio fluorescence sensing platform has high accuracy and reliability, and can be used for the analysis and detection of CQ in actual samples.

3.6. Method comparison

Compared with previously reported sensors for analyzing CQ activity (Table S3), this method possessed the following prominent features. (1) The LOD of this method (89.2 nM) was lower in comparison with most of the previously reported sensing strategies, which indicated superior sensitivity [12,13]. (2) The ratio fluorescent method has the inherent benefit of self-calibration correction for background environmental effects, which can significantly improve the sensing accuracy, and reliability for CQ detection. (3) This assay successfully avoided the complex synthesis and detection steps, which largely decreased the cost of the test and significantly streamlined the experiment processes. (4) A

portable test kit combined with a smartphone-based homemade 3D-printing portable device was developed for monitoring CQ for the first time, which provided a visual, equipment-free and portable tool for on-site detection of CQ.

4. Conclusion

In conclusion, a core-satellite nanostructure of AuNCs/CDs@SiO₂ was developed by confining AuNCs with the CDs@SiO₂ to creatively construct a ratio FL method for the determination of CQ. This study cased its distinctive characteristics as follows. (1) A straightforward and fast non-covalent electrostatic assembly technique was proposed as a means of synthesizing AuNCs/CDs@SiO₂, displaying increased fluorescence intensity of AuNCs with superior QY. (2) Leveraging the properties of AuNCs and CDs, as well as AuNCs' sensitivity to Cu²⁺, a creative ratio fluorescent analysis method for CQ detection was introduced, boasting an LOD of 89.2 nM. (3) A test kit for monitoring CQ was created, offering a tool that requires no additional equipment for on-site detection. The work is believed to provide not only insightful guidance for creating high-performance AuNCs/CDs@SiO₂-based composites, but also a practical means for monitoring CQ related drug residues monitoring. The limitation of this work is that the quantum yield of AuNCs is still not high, necessitating ongoing research endeavors that center on the development of AuNCs featuring notably elevated quantum yield.

CRedit authorship contribution statement

Yaqing Han: Software, Formal analysis, Data curation. **Mengke Wang:** Resources, Funding acquisition. **Junyang Chen:** Resources, Funding acquisition. **Guannan Wang:** Supervision, Project administration. **Shun Wang:** Writing – original draft, Supervision, Methodology, Funding acquisition, Formal analysis, Conceptualization. **Xia Zhao:** Investigation, Funding acquisition. **Haitao Han:** Data curation. **Yuze Chen:** Investigation. **Hao Wang:** Writing – review & editing, Data curation, Conceptualization.

Declaration of Competing Interest

The authors declare that they have no known competing financial interests or personal relationships that could have appeared to influence the work reported in this paper.

Acknowledgement

This project is supported by Shandong Provincial Natural Science Foundation, China (No. ZR2023QB145, No. ZR2023QB126, and No. ZR2022QB201), Traditional Chinese Medical Science and Technology Foundation of Shandong Province (No. Q-2023032), Opening Project of State Key Laboratory of Inorganic Synthesis and Preparative Chemistry in Jilin University (No. 2024-44, and No. 2024-25), and the Key R&D and Promotion Projects in Henan Province of China (242102311139).

Appendix A. Supporting information

Supplementary data associated with this article can be found in the online version at [doi:10.1016/j.snb.2024.137090](https://doi.org/10.1016/j.snb.2024.137090).

Data availability

Data will be made available on request.

References

- [1] F. Askarian, Z. Firoozi, A. Ebadollahi-Natanzi, S. Bahrami, H.R. Rahimi, A review on the pharmacokinetic properties and toxicity considerations for chloroquine and hydroxychloroquine to potentially treat coronavirus patients, *Toxicol. Res.* 38 (2022) 137–148.
- [2] W.Q. Ding, B.L. Liu, J.L. Vaught, H. Yamauchi, S.E. Lind, Anticancer activity of the antibiotic cloiquinol, *Cancer Res.* 65 (2005) 3389–3395.
- [3] D. Plantone, T. Koudriavtseva, Current and future use of chloroquine and hydroxychloroquine in infectious, immune, neoplastic, and neurological diseases: a mini-review, *Clin. Drug. Invest.* 38 (2018) 653–671.
- [4] T.S.K. Sharma, A. Ganguly, A. Santhan, K.Y. Hwa, Gadolinium oxide nanorods anchored on g-C₃N₄ nanosheets for dual-mode electrochemical determination of cloiquinol in real-time analysis, *ACS Appl. Nano Mater.* 5 (2022) 5208–5222.
- [5] G. Pedrioli, R. Patani, P. Paganetti, Chloroquine, the coronavirus crisis, and neurodegeneration: a perspective, *Front. Neurol.* 11 (2020) 596528.
- [6] H.C. Jiang, J.E. Taggart, X.X. Zhang, D.M. Benbrook, S.E. Lind, W.Q. Ding, Nitroxoline (8-hydroxy-5-nitroquinoline) is more a potent anti-cancer agent than cloiquinol (5-chloro-7-iodo-8-quinoline), *Cancer Lett.* 312 (2011) 11–17.
- [7] M.A.A. Al-Bari, Co-targeting of lysosome and mitophagy in cancer stem cells with chloroquine analogues and antibiotics, *J. Cell Mol. Med.* 24 (2020) 11667–11679.
- [8] B. Sriram, J.N. Baby, S.-F. Wang, M. George, X.B. Joseph, J.-T. Tsai, Surface engineering of three-dimensional-like hybrid AB₂O₄ (AB = Zn, Co, and Mn) wrapped on sulfur-doped reduced graphene oxide: investigation of the role of an electrocatalyst for cloiquinol detection, *ACS Appl. Electron. Mater.* 3 (2021) 362–372.
- [9] L.J. Xu, J.L. Sai, D.G. Xue, L. Zhou, R.J. Pei, A.H. Liu, Amplified peroxidase-like activity of Co²⁺ using 8-hydroxyquinoline and its application for ultrasensitive colorimetric detection of cloiquinol, *Chem. Asian J.* 16 (2021) 3957–3962.
- [10] J. Zhao, Z.F. Fan, Using zinc ion-enhanced fluorescence of sulfur quantum dots to improve the detection of the zinc(II)-binding antifungal drug cloiquinol, *Microchim. Acta* 187 (2020) 3.
- [11] G. Noe, Z. Amoura, D. Combarel, L. Lori, N. Tissot, A. Seycha, et al., Development and validation of a fast ultra-high performance liquid chromatography-fluorescent method for the quantification of hydroxychloroquine and its metabolites in patients with lupus, *Ther. Drug Monit.* 41 (2019) 476–482.
- [12] Q. Tan, X.X. An, S. Pan, S.J. Zhen, Y.M. Hu, X.L. Hu, One-pot hydrothermal method synthesis carbon dots as a fluorescent sensor for the sensitive and selective detection of cloiquinol, *Opt. Mater.* 123 (2022) 111830.
- [13] J. Wang, Y. Chang, P. Zhang, S.Q. Lie, P.F. Gao, C.Z. Huang, Cu²⁺-mediated fluorescence switching of gold nanoclusters for the selective detection of cloiquinol, *Analyst* 140 (2015) 8194–8200.
- [14] Y. Shu, Q.Y. Ye, T. Dai, Q. Xu, X.Y. Hu, Encapsulation of luminescent guests to construct luminescent metal-organic frameworks for chemical sensing, *ACS Sens.* 6 (2021) 641–658.
- [15] X.X. Luo, J.B. Liu, Ultrasmall luminescent metal nanoparticles: surface engineering strategies for biological targeting and imaging, *Adv. Sci.* 9 (2022) 2103971.
- [16] B.-B. Tao, N.-N. Wu, H.-D. Zhang, H.-B. Wang, Blocking the Cu (II) ions mediated catalytic ability for construction of ratiometric fluorescence sensing platform based on glutathione-stabilized copper nanoclusters, *J. Electrochem. Soc.* 169 (2022) 037529.
- [17] L. Yu, Y. Yang, X. Jiang, Y. Li, X. He, L. Chen, et al., A self-calibrating ratiometric fluorescence sensor with photonic crystal-based signal amplification for the detection of tetracycline in food, *Food Chem.* 451 (2024) 139418.
- [18] Y. Wang, J.Y. Jian, B.G. Sun, Y.L. Wei, D.D. Pan, J.X. Cao, et al., Engineering of onsite point-of-care testing of Fe³⁺ with visual ratiometric fluorescent signals of copper nanoclusters-driven portable smartphone, *Sens. Actuators B Chem.* 370 (2022) 132413.
- [19] L.G. Chen, J.J. Li, L. Sun, H.B. Wang, Ratiometric fluorometric assay triggered by alkaline phosphatase: proof-of-concept toward a split-type biosensing strategy for DNA detection, *Talanta* 271 (2024) 125703.
- [20] R.J. Gui, H. Jin, X.N. Bu, Y.X. Fu, Z.H. Wang, Q.Y. Liu, Recent advances in dual-emission ratiometric fluorescence probes for chemo/biosensing and bioimaging of biomarkers, *Coord. Chem. Rev.* 383 (2019) 82–103.
- [21] J. Chen, S. Jiang, M. Wang, X. Xie, X. Su, Self-assembled dual-emissive nanoprobes with metal-organic frameworks as scaffolds for enhanced ascorbic acid and ascorbate oxidase sensing, *Sens. Actuators B Chem.* 339 (2021) 129910.
- [22] Z.X. Han, N. Wang, Y.T. Lv, Q.J. Fu, G.N. Wang, X.G. Su, A novel self-assembled dual-emissive ratiometric fluorescent nanoprobes for alkaline phosphatase sensing, *Anal. Chim. Acta* 1287 (2024) 342146.
- [23] Z.T. Wei, W.Y. Lu, X.M. Wang, J.P. Ni, U.H. Prova, C.X. Wang, et al., Harnessing versatile dynamic carbon precursors for multi-color emissive carbon dots, *J. Mater. Chem. C* 10 (2022) 1932–1967.
- [24] Q. Xu, W.J. Li, L. Ding, W.J. Yang, H.H. Xiao, W.J. Ong, Function-driven engineering of 1D carbon nanotubes and 0D carbon dots: mechanism, properties and applications, *Nanoscale* 11 (2019) 1475–1504.
- [25] H. Kaurav, D. Verma, A. Bansal, D.N. Kapoor, S. Sheth, Progress in drug delivery and diagnostic applications of carbon dots: a systematic review, *Front. Chem.* 11 (2023) 1227843.
- [26] X.R. Xin, J.J. Liu, X.C. Liu, Y. Xin, Y.B. Hou, X.C. Xiang, et al., Melatonin-derived carbon dots with free radical scavenging property for effective periodontitis treatment via the Nrf2/HO-1 pathway, *ACS Nano* 18 (2024) 8307–8324.
- [27] H.B. Wang, Y. Li, H.Y. Bai, Y.M. Liu, DNA-templated Au nanoclusters and MnO₂ sheets: a label-free and universal fluorescence biosensing platform, *Sens. Actuators B Chem.* 259 (2018) 204–210.
- [28] J.C. Xiong, S. Zhang, L.Q. Qin, W.C. Shan, B.Y. Sun, J.Z. Shen, et al., Ultrasensitive inner filter effect fluorescence sensing platform for alkaline phosphatase based on arginine surface-engineered gold nanoclusters, *Sens. Actuators B Chem.* 378 (2023) 133177.
- [29] N.N. Wu, L.G. Chen, M.Z. Xiao, R.Y. Yuan, H.B. Wang, Determination of trypsin using protamine mediated fluorescent enhancement of DNA templated Au nanoclusters, *Microchim. Acta* 190 (2023) 158.
- [30] S. Niazi, I.M. Khan, W. Akhtar, F. ul Haq, I. Pasha, M.K.I. Khan, et al., Aptamer functionalized gold nanoclusters as an emerging nanoprobes in biosensing, diagnostic, catalysis and bioimaging, *Talanta* 268 (2024) 125270.
- [31] H.B. Wang, A.L. Mao, B.B. Tao, H.D. Zhang, Z.L. Xiao, Y.M. Liu, L-Histidine-DNA interaction: a strategy for the improvement of the fluorescence signal of poly (adenine) DNA-templated gold nanoclusters, *Microchim. Acta* 188 (2021) 198.
- [32] Y. Dong, H. Pang, H.B. Yang, C. Guo, J. Shao, Y. Chi, et al., Carbon-based dots co-doped with nitrogen and sulfur for high quantum yield and excitation-independent emission, *Angew. Chem. Int. Ed.* 52 (2013) 7800–7804.
- [33] W. Qin, J. Wang, Z. Tang, H. Tian, Z. Wu, Tris (2-carboxyethyl) phosphine-mediated immobilization of thiolated DNA on gold nanoclusters and its application in multiplex microRNA detection, *Sens. Actuators B Chem.* 401 (2024) 135028.
- [34] D.N. Li, R. Tan, X.N. Mi, C. Fang, Y.F. Tu, An electrochemiluminescent biosensor for noninvasive glucose detection based on cluster-like AuAg hollowed-nanoparticles, *Microchem. J.* 167 (2021) 106271.
- [35] J. Meng, E. Shuang, X. Wei, X.W. Chen, J.H. Wang, Confinement of AuAg NCs in a pomegranate-type silica architecture for improved copper ion sensing and imaging, *ACS Appl. Mater. Inter.* 11 (2019) 21150–21158.
- [36] R. Ma, L. Fu, N. Long, H. Guo, Y. Hou, Y. Li, et al., Gold nanoclusters and silica-coated carbon dots-assisted ratiometric fluorescent nanosensors for ultrasensitive detection of glyphosate, *ACS Sustain. Chem. Eng.* 11 (2023) 5093–5104.
- [37] V.A. Sadhu, S. Jha, V.N. Mehta, S.R. Miditana, T.J. Park, S.K. Kailasa, Green synthetic approach for the preparation of blue emitting gold nanoclusters: a simple analytical method for detection of hexaconazole fungicide, *J. Fluoresc.* (2024).
- [38] C. Chen, D. Zhao, B. Wang, P. Ni, Y. Jiang, C. Zhang, et al., Alkaline phosphatase-triggered in situ formation of silicon-containing nanoparticles for a fluorometric and colorimetric dual-channel immunoassay, *Anal. Chem.* 92 (2020) 4639–4646.
- [39] Z. Luo, X. Yuan, Y. Yu, Q. Zhang, D.T. Leong, J.Y. Lee, et al., From aggregation-induced emission of Au(I)-thiolate complexes to ultrabright Au(0)/Au(I)-thiolate core-shell nanoclusters, *J. Am. Chem. Soc.* 134 (2012) 16662–16670.

- [40] L. Luo, S.Q. Lin, Z.Y. Wu, H. Wang, Z.J. Chen, H. Deng, et al., Nanobody-based fluorescent immunoassay using carbon dots anchored cobalt oxyhydroxide composite for the sensitive detection of fenitrothion, *J. Hazard. Mater.* 439 (2022) 129701.
- [41] M. Wang, J. Zhang, X. Zhou, H. Sun, X. Su, Fluorescence sensing strategy for xanthine assay based on gold nanoclusters and nanozyme, *Sens. Actuators B Chem.* 358 (2022) 131488.
- [42] A. Li, H. Li, Y. Ma, T. Wang, X. Liu, C. Wang, et al., Bioinspired laccase-mimicking catalyst for on-site monitoring of thiram in paper-based colorimetric platform, *Biosens. Bioelectron.* 207 (2022) 114199.
- [43] M. Wang, X. Zhou, S. Wang, X. Xie, Y. Wang, X. Su, Fabrication of bioresource-derived porous carbon-supported iron as an efficient oxidase mimic for dual-channel biosensing, *Anal. Chem.* 93 (2021) 3130–3137.
- [44] M. Wang, L. Liu, X. Xie, X. Zhou, Z. Lin, X. Su, Single-atom iron containing nanozyme with peroxidase-like activity and copper nanoclusters based ratio fluorescent strategy for acetylcholinesterase activity sensing, *Sens. Actuators B Chem.* 313 (2020) 128023.
- [45] H.R. Liu, N.W. Zhu, M.T. Li, X.X. Huang, P.X. Wu, Z.L. Hu, et al., Induced fluorescent enhancement of protein-directed synthesized gold nanoclusters for selective and sensitive detection of flame retardants, *Sci. Total. Environ.* 713 (2020) 136488.
- [46] Z. Guo, G. Yu, Z. Zhang, Y. Han, G. Guan, W. Yang, et al., Intrinsic optical properties and emerging applications of gold nanostructures, *Adv. Mater.* 35 (2023) 2206700.
- [47] X.L. Bai, S.Y. Xu, L.Y. Wang, Full-range pH stable Au-clusters in nanogel for confinement-enhanced emission and improved sulfide sensing in living cells, *Anal. Chem.* 90 (2018) 3270–3275.
- [48] Y. Cai, H. Zhu, W. Zhou, Z. Qiu, C. Chen, A. Qileng, et al., Capsulation of AuNCs with AIE effect into metal-organic framework for the marriage of a fluorescence and colorimetric biosensor to detect organophosphorus pesticides, *Anal. Chem.* 93 (2021) 7275–7282.
- [49] J. Lu, C. Xu, Z. Tian, J. Lu, Y. Lin, Z. Shi, Green emission and Ag⁺ sensing of hydroxy double salt supported gold nanoclusters, *Nanoscale* 8 (2016) 5120–5125.
- [50] L. Wang, H.-X. Cao, Y.-S. He, C.-G. Pan, T.-K. Sun, X.-Y. Zhang, et al., Facile preparation of amino-carbon dots/gold nanoclusters FRET ratiometric fluorescent probe for sensing of Pb²⁺/Cu²⁺, *Sens. Actuators B-Chem.* 282 (2019) 78–84.
- [51] E. Babae, A. Barati, M.B. Gholivand, A. Taherpour, N. Zolfaghar, M. Shamsipur, Determination of Hg²⁺ and Cu²⁺ ions by dual-emissive Ag/Au nanocluster/carbon dots nanohybrids: switching the selectivity by pH adjustment, *J. Hazard. Mater.* 367 (2019) 437–446.
- [52] N. Guo, X. You, Y. Wu, D. Du, L. Zhang, Q. Shang, et al., Continuous fluorometric method for determining the monophenolase activity of tyrosinase on L-tyrosine, through quenching L-DOPA fluorescence by borate, *Anal. Chem.* 92 (2020) 5780–5786.

Shun Wang is a lecturer at College of Medical Engineering, Jining Medical University (China). He received her doctor's degree from Jilin University (China) in 2021. His research focuses on the application of nanozymes for biosensors.

Yaqing Han is currently carrying out her master's degree at College of Medical Engineering, Jining Medical University (China). Her research focuses on the synthesis and application of metal nanoclusters for sensing.

Mengke Wang is an associate professor at the College of Medical Engineering, Jining Medical University (China). Her research interests cover the synthesis the applications of fluorescent nanoprobe and nanozymes in biomedical sensing field.

Junyang Chen is an associate researcher at School of Life Sciences, Zhengzhou University. His research focuses on the synthesis, characterization, functionalization of metal-organic framework-based materials and their applications in biosensing.

Xia Zhao is a lecturer at College of Medical Engineering, Jining Medical University (China). Her research focuses on the theoretical and computational chemistry for biosensing.

Haitao Han is a lecturer at College of Medical Engineering, Jining Medical University (China). His research interests cover the synthesis of the nanozymes in-biomimetic enzyme catalysis.

Yuze Chen is pursuing his PhD study in Jilin University (China) under the guidance of professor Zhiqiang Liang. His research is mainly focused on the synthesis of covalent organic frameworks and their application on catalysis.

Hao Wang is a lecturer at College of Medical Engineering, Jining Medical University (China). His research focuses on the construction of sensor array for applications in early diagnosis of diseases.

Guannan Wang is currently a group leader and a full professor in the School of Pharmacy, Shenyang Medical College, China. He received his Ph.D in Analytical Chemistry from Jilin University, China, in 2011, as a postdoctoral researcher in 2012 under Pro Kajsa Uvdal in Linköping University. His research interests focus on bioactive materials, nanoprobe, and nanozymes used for bio-engineering, nanocatalysis, and sensing activity.